Exciton-polariton oscillations in real space

T. C. H. Liew,[1] Y. G. Rubo,[2] and A. V. Kavokin[3,4]

[1]*Division of Physics and Applied Physics, Nanyang Technological University, 637371 Singapore*

[2]*Instituto de Energías Renovables, Universidad Nacional Autónoma de México, Temixco, Morelos 62580, Mexico*

[3]*Russian Quantum Center, 100 Novaya Street, Skolkovo, Moscow Region 143025, Russia*

[4]*Physics and Astronomy School, University of Southampton, Highfield, Southampton SO171BJ, United Kingdom*

(Received 14 August 2014; revised manuscript received 16 December 2014; published 29 December 2014)

We introduce and model spin-Rabi oscillations based on exciton-polaritons in semiconductor microcavities. The phase and polarization of oscillations can be controlled by resonant coherent pulses and the propagation of oscillating domains gives rise to phase-dependent interference patterns in real space. We show that interbranch polariton-polariton scattering controls the propagation of oscillating domains, which can be used to realize logic gates based on an analog variable phase.

DOI: 10.1103/PhysRevB.90.245309 PACS number(s): 71.36.+c, 42.65.Sf, 42.65.Yj, 78.67.−n

I. INTRODUCTION

Rabi oscillations are well known for their role in nuclear magnetic resonance devices, and they underly proposals for quantum computing [1,2]. Following the archetypical example of coherent and reversible energy transfer between atoms and light in electromagnetic cavities [3], Rabi oscillations have been achieved at the quantum level in a variety of systems, including Josephson junctions [4,5], electron spins in quantum dots [6,7], nuclear spin systems [8] and molecular magnets [9].

Rabi oscillations were also observed in planar semiconductor systems, such as quantum wells containing excitons [10], and semiconductor microcavities containing exciton-polaritons [11,12]. Conversion of spin-polarized excitons into circularly polarized photons and vice versa in microcavities results in magnetization oscillations with terahertz frequencies [13]. Planar microcavities also allow the ballistic transport of energy in space [14], with exciton-polaritons covering distances on the order of hundreds of microns [15,16]. While Josephson oscillations [17,18] and other spatially dependent oscillations [19] were reported recently, the study of exciton-polariton Rabi oscillations has been typically kept separate from the study of spatial dynamics. The interplay between Rabi and Josephson oscillations was discussed in the recent theoretical work of Voronova, Elistratov, and Lozovik [20], while the real space dynamics was not discussed. Real space dynamics is usually separated from Rabi oscillations due to the fact that Rabi oscillations are short-lived, surviving only a limited number of cycles due to the short polariton lifetime (a few tens of picoseconds in state-of-the-art samples). Nevertheless propagating polaritons have been progressing steadily toward the realization of optical circuits, where their light effective mass and strong nonlinear interactions have allowed several implementations of optical switches [21–23] and transistors [24,25].

To overcome the limited duration of Rabi oscillation, one can consider the amplification [15] of polaritons by a nonresonant excitation. This creates a reservoir of hot excitons, which can undergo stimulated scattering into polariton states. The result is an effective incoherent pumping or gain mechanism of polariton states, which can compensate polariton decay [26]. Using a Ginzburg-Landau type model [27] we show that this results in sustained Rabi oscillations, which brings new opportunities for their control, manipulation and application.

Exciton-polaritons also have a rich spin dynamics [28], allowed by their two-component spin degree of freedom. We show that the propagation of polariton spin oscillations induced by Rabi oscillations [13] in space can be influenced by applied magnetic fields, as well as transverse electric–transverse magnetic (TE-TM) splitting of the modes. We show that Rabi oscillations can be further controlled by applying additional pulses to the system, which may enhance or suppress oscillations, where the pulse phase becomes a control variable.

Finally, we consider oscillations between exciton-polariton states with different momenta (i.e., different in-plane wave vectors), where propagating domains in real space are distinguished by their phase. In analogy to previous studies of domain wall propagation [29,30], the domains act as information carriers and logic gates can be realized from the combination of domains at engineered points of space. However, unlike previous work, the phase of the domains is a free continuous variable, opening an area of analog information processing in polaritonics.

II. THEORETICAL MODEL

To describe a coherent state of excitons and cavity photons, we introduce the mean-field wave functions [31] of spin-polarized excitons, χ_σ, and photons, ϕ_σ. The index $\sigma = \pm$ accounts for the two possible spin projections of (optically active) excitons and photons on the structure growth axis. The evolution of the mean-fields is described by complex Ginzburg-Landau equations [27,32]:

$$i\hbar\frac{\partial\chi_\sigma}{\partial t} = [E_X + \sigma\Omega_Z + i(P_\sigma - \Gamma_X - \Gamma_{\rm NL}|\chi_\sigma|^2) + \alpha_1|\chi_\sigma|^2 + \alpha_2|\chi_{-\sigma}|^2]\chi_\sigma + \Omega\phi_\sigma, \quad (1)$$

$$i\hbar\frac{\partial\phi_\sigma}{\partial t} = \left(-\frac{\hbar^2}{2m_C}\hat{\nabla}^2 - i\Gamma_C\right)\phi_\sigma + \Omega\chi_\sigma + F_\sigma. \quad (2)$$

Here E_X represents the exciton-photon detuning and we neglected the dispersion of excitons, which is flat compared to the parabolic photon dispersion given by the light photon effective mass m_C. In a magnetic field excitons experience a

Zeeman splitting [28], given by $2\Omega_Z$. The incoherent pumping of the system is described by the polarized [16] pumping strength P_σ, which is saturated at high densities due to nonlinear losses [27] characterized by $\Gamma_{\rm NL}$. We also allow for a coherent resonant pumping with amplitude F_σ. Γ_X and Γ_C are the decay rates of excitons and photons, respectively. Nonlinear interactions between excitons are introduced in Gross-Pitaevskii form [31], where α_1 and α_2 represent the strengths of interactions between parallel and antiparallel spins, respectively. Finally, Ω is the Rabi coupling strength between the excitons and photons.

It is worth noting that, from the three nonlinear parameters in Eqs. (1) and (2), the solution depends only on the ratios α_2/α_1 and $\Gamma_{\rm NL}/\alpha_1$ up to an overall amplitude. This can be seen by substituting the scaled quantities $\chi' = \sqrt{\alpha_1}\chi$, $\phi' = \sqrt{\alpha_1}\phi$, and $F' = \sqrt{\alpha_1}F$. Consequently, we will not set α_1 explicitly, but set $\alpha_2 = -0.1\alpha_1$ (see Ref. [33]) and $\Gamma_{\rm NL} = 0.3\alpha_1$ (see Ref. [27]) in our calculations.

III. HOMOGENEOUS SOLUTIONS

To gain some understanding of the states supported by Eqs. (1) and (2), let us first consider a spatially homogeneous incoherent pumping and no coherent pumping ($F_\sigma = 0$). For simplicity, let us also first neglect the Zeeman splitting, exciton-photon detuning ($E_X = 0$), and polariton-polariton interaction terms ($\Omega_Z = 0; \alpha_1 = 0, \alpha_2 = 0$). For pump powers exceeding a threshold $P \geqslant P_{\rm th} = \Gamma_C + \Gamma_X$, stationary homogeneous states exist:

$$\phi_\sigma = \frac{\Omega\chi_\sigma}{\hbar\mu + i\Gamma_C}, \quad \chi_\sigma = \sqrt{\frac{P_\sigma - \Gamma_C - \Gamma_X}{\Gamma_{\rm NL}}}e^{-i\mu t + i\theta_\sigma}, \quad (3)$$

where $\hbar\mu = \sqrt{\Omega^2 - \Gamma_C^2}$. Since there are no terms coupling σ^+ and σ^- polarized states in Eqs. (1) and (2), we effectively have two scalar problems. This would not be the case in the presence of a polarization splitting; however, let us first consider homogeneous states with zero in-plane wave vector, where TE-TM splitting is zero and we neglect sample anisotropy. Note that the incoherent pumping does not fix the phase of the solutions, given by θ_σ, which would be set by initial excitation conditions. The stability of the stationary solution can be checked by considering the spectrum of elementary excitations [31]. While the solution (3) is stable, it is not the only possibility.

We may also consider oscillating solutions of the form $\chi_\sigma(t) = \chi_{\sigma,1}\sin(\omega t)$ and $\phi_\sigma(t) = i\phi_{\sigma,1}\sin(\omega t) + i\phi_{\sigma,2}\cos(\omega t)$, where $\chi_{\sigma,1}, \phi_{\sigma,1}$, and $\phi_{\sigma,2}$ are taken to be constants. Substituting into Eqs. (1) and (2), and collecting terms oscillating as $\cos(\omega t)$ and $\sin(\omega t)$, we obtain the approximate solution

$$\phi_{\sigma,1} = -\frac{\Omega\Gamma_C}{(\hbar\omega)^2 + \Gamma_C^2}\chi_{\sigma,1}, \quad \phi_{\sigma,2} = \frac{\hbar\omega}{\Omega}\chi_{\sigma,1},$$
$$|\chi_{\sigma,1}|^2 = \frac{2}{3}\frac{(P - \Gamma_C - \Gamma_X)}{\Gamma_{\rm NL}}, \quad \hbar\omega = \pm\sqrt{\Omega^2 - \Gamma_C^2}. \quad (4)$$

Here we neglected fast oscillating terms proportional to $\sin(3\omega t)$, appearing in the expansion of the term $\sin^3(\omega t) = [3\sin(\omega t) - \sin(3\omega t)]$. A comparison with the direct numerical solution of Eqs. (1) and (2) is shown in Fig. 1(a).

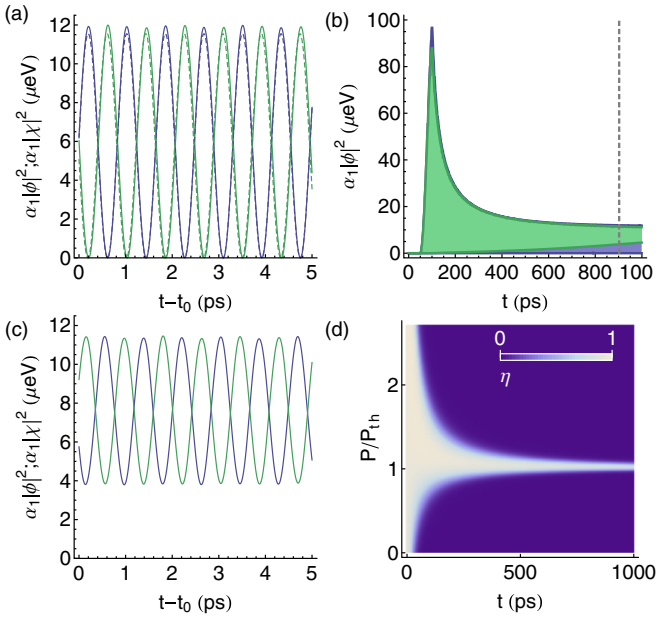

FIG. 1. (Color online) (a) Homogeneous oscillating solutions for the photon and exciton intensity, $|\phi(t)|^2$ and $|\chi(t)|^2$, respectively in the case of a scalar condensate (circularly polarized excitation) in the absence of polariton-polariton interactions. Solid curves show numerically obtained results via the application of a pulse to the system. Superimposed dashed curves show the approximate analytical result. (b) Long term dynamics of the envelope of $|\phi(t)|^2$ when excited by a short pulse. At long times the presence of interactions slowly reduces the amplitude of oscillations, as shown by the green (light gray) envelope. In the absence of interactions, the oscillations would persist, as shown by the blue (dark gray) envelope. Note that the blue (dark gray) envelope is overlapped by the green (light gray) envelope at short times. (c) Same as in (a) but including interactions. The oscillations are shown for the time represented by the vertical line in (b). (d) Visibility of the Rabi oscillations, for different pump intensities as a function of time. Parameters: $\Omega = 2.5$ meV, $\hbar/\Gamma_C = 10$ ps, $\hbar/\Gamma_X = 100$ ps, $P = 0.075$ meV, $\Omega_Z = 0$.

To place the system in an oscillating state a 50 ps pulse $F_\sigma(t)$ modulated at frequency $\hbar\omega$ was applied to the photon evolution according to Eq. (2), where the long-term evolution is shown by the envelope function in Fig. 1(b). The numerical calculation is made with an initial zero amplitude condition for the exciton and photon fields; the condensate is then seeded by the coherent pulse.

It is worth noting that in the work of Ref. [12] an additional dephasing of upper polaritons was inferred from experimental data. We believe this extra dephasing was a result of a short (100 fs) pulse, resulting in a broad energy (few meV) population of lower and upper polaritons. Despite the presence of spectral filtering, the population of multiple energies would automatically induce dephasing via multiple polariton scattering in reciprocal space (when spatial dynamics is fully accounted). In the present manuscript, we consider pulses of longer duration and consequently do not account for additional upper polariton dephasing (while we will account fully for spatial dynamics in the following sections). We nevertheless point out that the presence of any dephasing would have a strong limitation on the lifetime of Rabi oscillations.

The Rabi oscillations are destroyed on long timescales. The phase difference between the exciton and photon component is $\pi/2$ at any moment of time for the Rabi oscillating solution. Fluctuations of the phase difference away from this value will lead to decay of oscillations. There are two sources of dephasing in this system. The first appears because of the noise from the excitonic reservoir, that always accompanies the presence of incoherent pump [34,35]. The second source is due to interactions. The inclusion of nonlinear interaction terms α_1 and α_2 at the first-order mean-field level is sufficient to generate the dephasing and decay of oscillations. This decay is illustrated by comparison of the blue and green envelopes in Fig. 1(b) as well as the reduced oscillation amplitudes shown at short timescales in Fig. 1(c). The oscillation decay time shortens with larger polariton densities. Defining the visibility of Rabi oscillations as $\eta = (I_{\max} - I_{\min})/(I_{\max} + I_{\min})$, where $I_{\max}$ and $I_{\min}$ are the maximum and minimum values of $|\phi(t)|^2$ in an oscillation cycle, respectively, Fig. 1(d) illustrates the dependence of the decay of Rabi oscillations on the pump power. If we work in a regime near the condensation threshold then the decay time remains very long, where the oscillations are sustained long after the pulse has passed, with a decay time greatly exceeding the polariton lifetime.

Given that the two spin polarized components are decoupled, it is possible to prepare them in different states. Pairing a linearly polarized nonresonant (effectively incoherent) pump ($P_+ = P_-$) with a circularly polarized pulse $F_+(t)$ excites Rabi oscillations in the σ^+ polarization, while the σ^- polarization achieves the stationary state given by Eq. (3). Such a situation is shown in Fig. 2(a) (which includes also the slow decay of oscillations caused by nonlinear interactions). In this way, the presence of Rabi oscillations also manifests in a circular rotation of the pseudospin vector [28] on the Poincaré sphere [Fig. 2(b)]. In contrast to common expectations, this pseudospin rotation is not related to any polarization splitting.

It can be noted that in separate numerical calculations the presence of a finite magnetic field $\Omega_Z \neq 0$ and/or finite exciton-photon detuning $E_X \neq 0$ was found to have little effect on the observed phenomenology, while the oscillation frequency $\hbar\omega$ may become slightly modified.

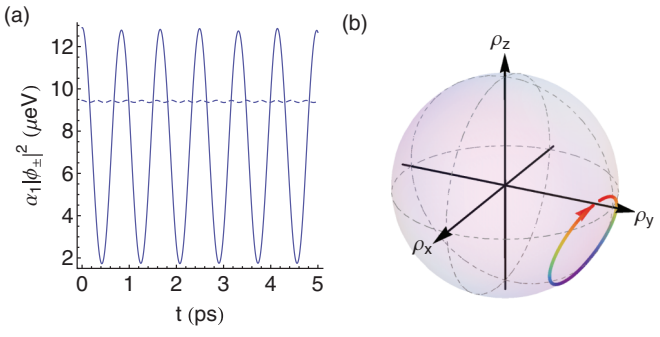

FIG. 2. (Color online) (a) Under a linearly polarized nonresonant pump, a circularly polarized pulse generates exciton-photon Rabi oscillations in one circularly polarized component while the other component maintains a fixed intensity. (b) Pseudospin evolution in the Poincaré sphere. The parameters were taken the same as in Fig. 1 with $\alpha_2 = -0.1\alpha_1$.

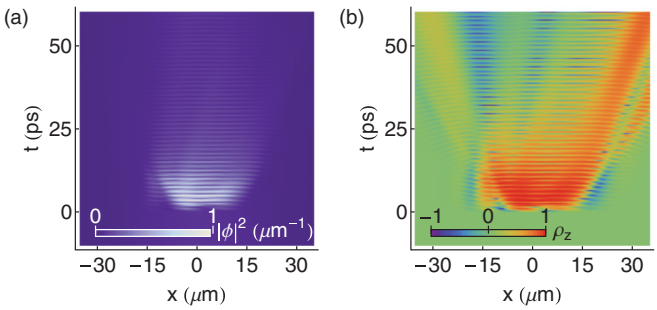

FIG. 3. (Color online) (a) Spatial dynamics of a polariton condensate excited by a linearly polarized nonresonant pump. A circularly polarized pulse with nonzero in-plane wave vector induces propagating Rabi oscillations, beginning at $t = 0$ ps. (b) Associated dynamics of the circular polarization degree. Parameters were the same as in Fig. 1 (in the presence of nonlinear interactions) with $P_0 = 0.1$ meV, $m_C = 7.5\times10^{-5} m_e$ and $k_F = 0.5$ μm^{-1}.

IV. SPATIAL PROPAGATION OF RABI OSCILLATIONS

If the applied coherent pulse is not homogeneous in space, but rather localized, then one can consider the resulting propagation of the induced spin-Rabi oscillations. Figure 3 shows results from the numerical solution of Eqs. (1) and (2) using a broad Gaussian shaped incoherent cw excitation and a focused Gaussian shaped pulse. Fast oscillations can again be observed in the total polariton intensity ($|\phi_+|^2 + |\phi_-|^2$) and circular polarization degree. However, the introduction of a nonzero in-plane wave vector of the pulse [i.e., modulation of F_+ by $\exp(ik_F x)$] induces the spatial propagation of oscillations, which continue toward the edge of the incoherent pump even after the pulse has passed. The nonzero value of k_F can also be seen as responsible for the generation of an asymmetric intensity and polarization distribution in x. The spreading of an oscillating nonuniform spin polarization is further illustrated by several snapshots of the spatial distribution of the circular polarization degree shown in Fig. 4. Due to the dispersion of polaritons, a slightly higher pump power than that considered in Figs. 1 and 2 was required to achieve threshold. This caused a larger typical polariton

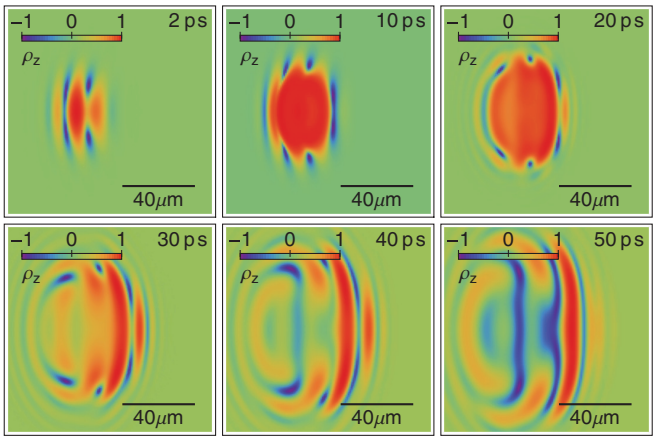

FIG. 4. (Color online) Snapshots of the spatial distribution of the circular polarization degree at selected times, showing the propagation of Rabi oscillations corresponding to Fig. 3.

density, resulting in a faster decay of Rabi oscillations, which remain visible over a timescale of ∼300 ps.

It is worth noting that kinetic energy relaxation of propagating polaritons has been observed in a variety of nonresonantly excited experiments [15,36]. While we have shown that Rabi oscillations do not require kinetic energy for their existence, the relaxation of kinetic energy may limit their propagation distance in an experiment.

A. Influence of TE-TM splitting on propagating spin-Rabi oscillations

Many semiconductor microcavities exhibit an additional k-dependent polarization splitting, mainly due to the different energies of transverse electric (TE) and transverse magnetic (TM) photonic cavity modes. This splitting is well known to influence the spin dynamics and resulting spatial patterns formed by propagating polaritons (see, e.g., [16,28,37] and references within).

Theoretically, the TE-TM splitting can be accounted for by adding a wave vector dependent term that couples the two spin components to the right-hand side of Eq. (2):

$$i\hbar\frac{\partial\phi_\sigma}{\partial t} = \cdots + \frac{\Delta_{\mathrm{LT}}}{k_{\mathrm{LT}}^2}\left(i\frac{\partial}{\partial x} + \sigma\frac{\partial}{\partial y}\right)^2\phi_{-\sigma} \qquad (5)$$

where Δ_{LT} determines the strength of the TE-TM splitting at the in-plane wave vector k_{LT}.

For typical parameters, we obtain the result shown in Fig. 5. The basic phenomenology of propagating spin-Rabi oscillations remains; however, the TE-TM splitting breaks the mirror symmetry of the system about the horizontal axis. This gives rise to asymmetric patterns in the distribution of the circular polarization degree. The breaking of the system symmetry is a consequence of the TE-TM splitting acting on an initial preferred polarization direction [38].

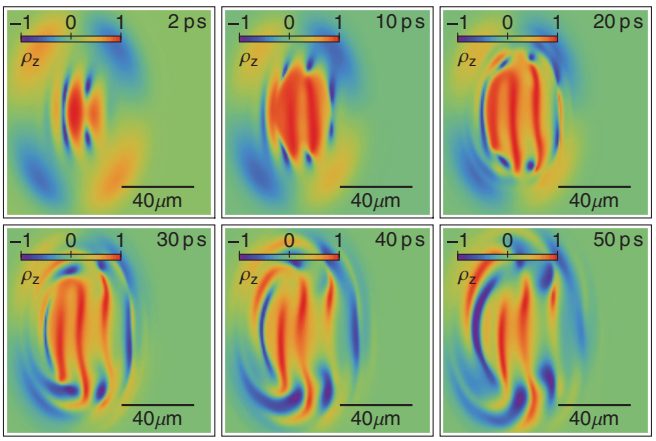

FIG. 5. (Color online) Influence of TE-TM splitting, giving rise to an asymmetric spatial distribution of Rabi oscillations. Images show the same as in Fig. 4, accounting for TE-TM splitting. Parameters: $\Delta_{\mathrm{LT}} = 0.1$ meV, $k_{\mathrm{LT}} = 1\,\mu\mathrm{m}^{-1}$, $\Omega_Z = 0$ meV.

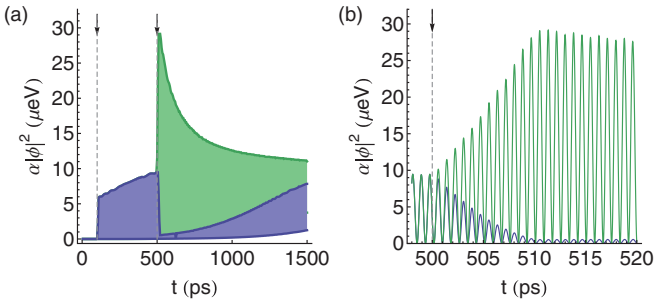

FIG. 6. (Color online) Effect of two pulses on the scalar homogeneous system. An initial pulse at $t = 100$ ps (marked by an arrow) induces Rabi oscillations in the system. An additional pulse is applied at $t = 500$ ps (marked by another arrow), which is either in phase (blue/dark gray) or out-of phase (green/light gray) with the Rabi oscillations. The in-phase pulse causes a temporary amplification of oscillations while the out-of-phase pulse suppresses the oscillations, which return after a delay. Parameters were the same as in Fig. 1 (in the presence of nonlinear interactions).

V. TWO-PULSE EXCITATION

A. Homogeneous case

Let us now return to considering the homogeneously excited scalar system (considering separately a particular spin component). Figure 6 shows the time evolution of the photon intensity $|\phi|^2$ when subjected to a pair of pulses arriving at times indicated by the arrows and vertical dashed lines. The first pulse induces Rabi oscillations in the system, which reach a fixed maximum amplitude (as seen before in Fig. 1). The second pulse can either amplify or suppress the oscillations, depending on whether it is in phase or out of phase with the global photon phase of the oscillations. In the former case, the amplification decays quickly, on the order of the polariton lifetime. In the case of an out-of-phase second pulse, the Rabi oscillations in the system can be suppressed for an extended period, with careful tuning of the pulse amplitude. While we included the effect of polariton-polariton interactions in our calculation, this was only for completeness, and similar results are obtained also in the hypothetical case of $\alpha_{1,2} = 0$.

B. Interactions between propagating Rabi domains

In the case of spatially separated pulses, with Gaussian spatial profiles, it is possible to observe collisions between propagating Rabi domains. In Fig. 7, two Rabi oscillating domains are generated by a pair of pulses arriving at $t = 0$ ps. The pulses set the photon (and exciton) phase of their respective domains, and the resulting interference pattern of the domains differs depending on whether the pulses arrive in phase [Figs. 7(a) and 7(b)], where one has constructive interference at $x = 0$, or out of phase [Figs. 7(c) and 7(d)], where one has destructive interference at $x = 0$. Remarkably, the phase difference between the two domains is maintained for long times at which the pulses have decayed and the system is only fed by the nonresonant pump, which has no direct control on the system phase.

This phase sensitivity of interfering polaritons has previously been appreciated as an ingredient for polaritonic

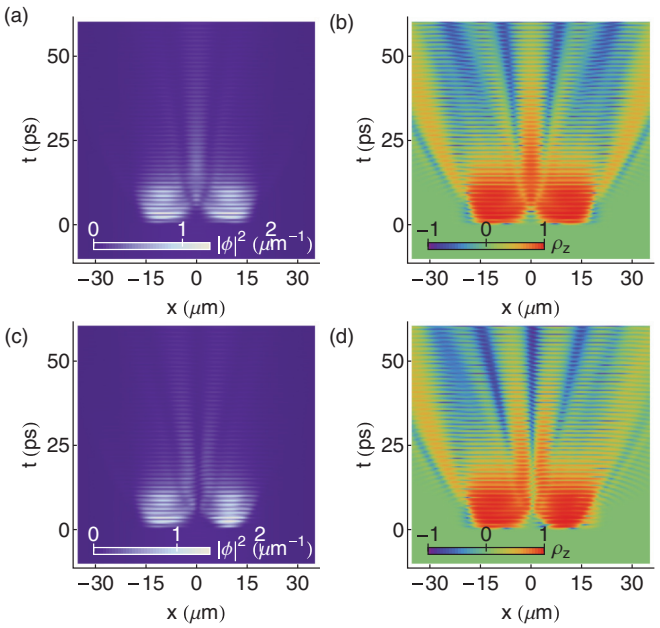

FIG. 7. (Color online) Interference of Rabi oscillations generated by two spatially separated pulses. Each pulse arrives at the same time, within the area of a background Gaussian shaped incoherent continuous wave pump. Panels (a) and (b) show the evolution of the total intensity and circular polarization degree, respectively, for in-phase pulses. Panels (c) and (d) show the same for out-of-phase pulses. Parameters were the same as in Fig. 3. The two pulses have equal and opposite wave vectors, $k_F = \pm 0.5\ \mu\mathrm{m}^{-1}$, and are shifted by $x = \mp 10\ \mu\mathrm{m}$, respectively, from the center of the incoherent pump.

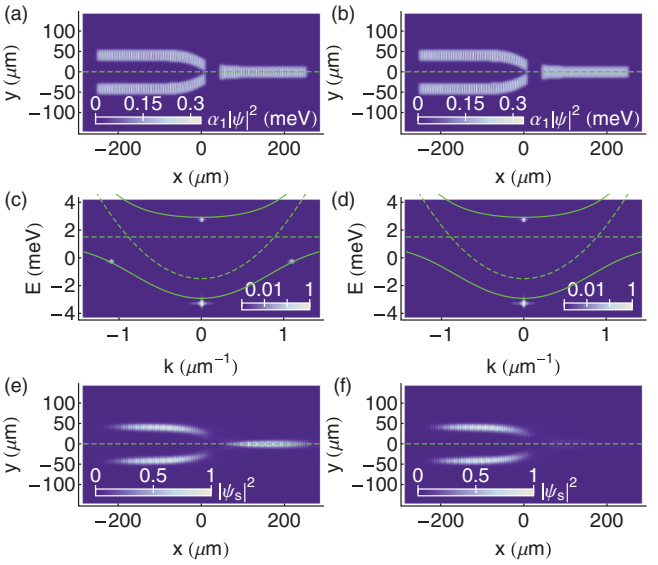

FIG. 8. (Color online) Interference of parametric oscillations in polariton channels formed by spatial patterning of the pumping field $F(x)$. Panels (a) and (b) show the intensity distribution of polaritons 200 ps after the arrival of a pair of input pulses applied to the left-hand channels with the same and opposite phases, respectively. Panels (c) and (d) show the polariton dispersions along the horizontal dashed lines in (a) and (b), respectively. Dashed curves represent the bare exciton (flat) and photon dispersion, while solid curves show the lower and upper polariton branches. Panels (e) and (f) show the polariton signal intensity, obtained by filtering around the wave vector $k_s \approx 1.05\ \mu\mathrm{m}^{-1}$) in (c) and (d), respectively.

information processing [39]. The spreading of Rabi oscillating domains is also reminiscent of spin polarized domains, which can be used to realize binary logic gates [29]. However, a limitation of the propagation shown in Fig. 3 is that it occurs only in one direction: the one set by the wave vector of the applied pulse. For the construction of cascadable logic gates, one typically needs to have signals capable of traveling in a variety of directions in the microcavity plane.

VI. PARAMETRIC OSCILLATIONS AND ANALOG LOGIC IN REAL SPACE

To allow for oscillating domains that propagate in all directions, we make use of the potential parametric scattering [40] between polariton modes, allowed by the nonlinear α-dependent term in Eq. (1). Considering the simultaneous coherent excitation of the bottom of the lower and upper polariton branches, one can expect scattering to nonzero wave vector states on the lower polariton branch [41], as demonstrated in Fig. 8(c) (this requires a positive exciton-photon detuning; $E_X = 3$ meV).

By the spatial patterning of the pumping field $F(x)$, one can confine polaritons along channels and we consider a "Y"-shaped channel in Fig. 8. Applied pulses localized in the left-hand channels trigger the parametric scattering and also set the phase of the resulting signal states. Figure 8(a) shows the polariton intensity 200 ps after the pulses arrive, which are chosen to have the same phase (for simplicity, we consider only a single spin component here). A weak spatial modulation of the polariton density is associated with the scattering in reciprocal space shown in Fig. 8(c). Filtering of the polariton field around the signal wave vector ($k_s \approx 1.05\ \mu\mathrm{m}^{-1}$) clearly shows that the signal has propagated into the right-hand output channel.

In contrast, when pulses excite signals in the channels with opposite phase, they interfere destructively at the point where channels join, suppressing the propagation.

A further advantage of this scheme is that the signal wave vector can be tuned near the point of maximum group velocity of the lower polariton dispersion. In principle, this allows repetition rates of the order of tens of gigahertz, which could be further improved by reducing the dimensions of the channel pattern. On the other hand, oscillating parametric polariton solitons [42,43] with very different spatial profiles and frequencies can be obtained operating near a flatter exciton-like region of the dispersion.

VII. CONCLUSION

We considered the generation of exciton-polariton Rabi oscillating domains in semiconductor microcavities subjected to coherent pulses. A continuous wave incoherent pump compensates the polariton lifetime, giving rise to sustained oscillations. The spin polarization of oscillations can be

selected via the pulse polarization, which also allows the generation of terahertz frequency oscillations in the polariton spin degree of freedom. The oscillations remain in the presence of magnetic fields or TE-TM splitting, and can be further controlled by the application of additional pulses.

An important property of the Rabi domains is that their phase can be varied, which gives a continuous variable for encoding information. By making use of interbranch polariton-polariton scattering, the propagation of oscillating domains can be controlled along channels by patterning the incident optical field. A logical phase-dependent behavior is observed from the interference when domains collide. This opens a route for analog architectures in polaritonic devices.

ACKNOWLEDGMENTS

We are indebted to D. Sanvitto, F. Laussy, A. Alodjants, I. A. Shelykh, and K. Kristinsson for fruitful discussions. Y.G.R. and A.V.K. acknowledge support from the EU FP7 IRSES Project POLAPHEN. A.V.K. also acknowledges support from an EPSRC fellowship. T.L. acknowledges support from the Lee Kuan Yew Endowment Fund.

[1] J. I. Cirac and P. Zoller, Phys. Rev. Lett. **74**, 4091 (1995).
[2] D. R. Leibrandt, J. Labaziewicz, R. J. Clark, I. L. Chuang, R. J. Epstein, C. Ospelkaus, J. H. Wesenberg, J. J. Bollinger, D. Leibfried, D. J. Wineland, D. Stick, J. Sterk, C. Monroe, C. S. Pai, Y. Low, R. Frahm, and R. E. Slusher, Quantum Inf. Comput. **9**, 901 (2009).
[3] Y. Kaluzny, P. Goy, M. Gross, J. M. Raimond, and S. Haroche, Phys. Rev. Lett. **51**, 1175 (1983).
[4] J. M. Martinis, S. Nam, J. Aumentado, and C. Urbina, Phys. Rev. Lett. **89**, 117901 (2002).
[5] Y. Yu, S. Y. Han, X. Chu, S. I. Chu, and Z. Wang, Science **296**, 889 (2002).
[6] J. R. Petta, A. C. Johnson, J. M. Taylor, E. A. Laird, A. Yacoby, M. D. Lukin, C. M. Marcus, M. P. Hanson, and A. C. Gossard, Science **309**, 2180 (2005).
[7] F. H. L. Koppens, C. Buizert, K. J. Tielrooij, I. T. Vink, K. C. Nowack, T. Meunier, L. P. Kouwenhoven, and L. M. K. Vandersypen, Nature (London) **442**, 766 (2006).
[8] F. Jelezko, T. Gaebel, I. Popa, M. Domhan, A. Gruber, and J. Wrachtrup, Phys. Rev. Lett. **93**, 130501 (2004).
[9] J. Yang, Y. Wang, Z. Wang, X. Rong, C. K. Duan, J. H. Su, and J. Du, Phys. Rev. Lett. **108**, 230501 (2012).
[10] A. Schülzgen, R. Binder, M. E. Donovan, M. Lindberg, K. Wundke, H. M. Gibbs, G. Khitrova, and N. Peyghambarian, Phys. Rev. Lett. **82**, 2346 (1999).
[11] T. B. Norris, J. K. Rhee, C. Y. Sung, Y. Arakawa, M. Nishioka, and C. Weisbuch, Phys. Rev. B **50**, 14663 (1994).
[12] L. Dominici, D. Colas, S. Donati, J. P. Restrepo Cuartas, M. De Giorgi, D. Ballarini, G. Guirales, J. C. López Carreño, A. Bramati, G. Gigli, E. del Valle, F. P. Laussy, and D. Sanvitto, Phys. Rev. Lett. **113**, 226401 (2014).
[13] A. Brunetti, M. Vladimirova, D. Scalbert, M. Nawrocki, A. V. Kavokin, I. A. Shelykh, and J. Bloch, Phys. Rev. B **74**, 241101 (2006).
[14] A. A. High, A. T. Hammack, J. R. Leonard, Sen Yang, L. V. Butov, T. Ostatnicky, M. Vladimirova, A. V. Kavokin, T. C. H. Liew, K. L. Campman, and A. C. Gossard, Phys. Rev. Lett. **110**, 246403 (2013).
[15] E. Wertz, A. Amo, D. D. Solnyshkov, L. Ferrier, T. C. H. Liew, D. Sanvitto, P. Senellart, I. Sagnes, A. Lemaître, A. V. Kavokin, G. Malpuech, and J. Bloch, Phys. Rev. Lett. **109**, 216404 (2012).
[16] E. Kammann, T. C. H. Liew, H. Ohadi, P. Cilibrizzi, P. Tsotsis, Z. Hatzopoulos, P. G. Savvidis, A. V. Kavokin, and P. G. Lagoudakis, Phys. Rev. Lett. **109**, 036404 (2012).
[17] K. G. Lagoudakis, B. Pietka, M. Wouters, R. Andre, and B. Deveaud-Pledran, Phys. Rev. Lett. **105**, 120403 (2010).
[18] M. Abbarchi, A. Amo, V. G. Sala, D. D. Solnyshkov, H. Flayac, L. Ferrier, I. Sagnes, E. Galopin A. Lemaître, G. Malpuech, and J. Bloch, Nat. Phys. **9**, 275 (2013).
[19] M. De Giorgi, D. Ballarini, P. Cazzato, G. Deligeorgis, S. I. Tsintzos, Z. Hatzopoulos, P. G. Savvidis, G. Gigli, F. P. Laussy, and D. Sanvitto, Phys. Rev. Lett. **112**, 113602 (2014).
[20] N. S. Voronova, A. A. Elistrativ, and Yu. E. Lozovik, arXiv:1411.2346.
[21] A. Amo, T. C. H. Liew, C. Adrados, R. Houdré, E. Giacobino, A. V. Kavokin, and A. Bramati, Nat. Photon. **4**, 361 (2010).
[22] C. Adrados, T. C. H. Liew, A. Amo, M. D. Martín, D. Sanvitto, C. Antón, E. Giacobino, A. Kavokin, A. Bramati, and L. Viña, Phys. Rev. Lett. **107**, 146402 (2011).
[23] M. De Giorgi, D. Ballarini, E. Cancellieri, F. M. Marchetti, M. H. Szymanska, C. Tejedor, R. Cingolani, E. Giacobino, A. Bramati, G. Gigli, and D. Sanvitto, Phys. Rev. Lett. **109**, 266407 (2012).
[24] T. Gao, P. S. Eldridge, T. C. H. Liew, S. I. Tsintzos, G. Stavrinidis, G. Deligeorgis, Z. Hatzopoulos, and P. G. Savvidis, Phys. Rev. B **85**, 235102 (2012).
[25] D. Ballarini, M. De Giorgi, E. Cancellieri, R. Houdre, E. Giacobino, R. Cingolani, A. Bramati, G. Gigli, and D. Sanvitto, Nat. Commun. **4**, 1778 (2013).
[26] S. S. Demirchyan, I. Y. Chestnov, A. P. Alodjants, M. M. Glazov, and A. V. Kavokin, Phys. Rev. Lett. **112**, 196403 (2014).
[27] J. Keeling and N. G. Berloff, Phys. Rev. Lett. **100**, 250401 (2008).
[28] I. A. Shelykh, Y. G. Rubo, A. V. Kavokin, T. C. H. Liew, and G. Malpuech, Semicond. Sci. Technol. **25**, 013001 (2010).
[29] T. C. H. Liew, A. V. Kavokin, and I. A. Shelykh, Phys. Rev. Lett. **101**, 016402 (2008).
[30] T. Espinosa-Ortega and T. C. H. Liew, Phys. Rev. B **87**, 195305 (2013).
[31] I. Carusotto and C. Ciuti, Phys. Rev. Lett. **93**, 166401 (2004).
[32] M. Wouters and I. Carusotto, Phys. Rev. Lett. **99**, 140402 (2007).
[33] D. N. Krizhanovskii, D. Sanvitto, I. A. Shelykh, M. M. Glazov, G. Malpuech, D. D. Solnyshkov, A. Kavokin, S. Ceccarelli, M. S. Skolnick, and J. S. Roberts, Phys. Rev. B **73**, 073303 (2006).
[34] D. Read, T. C. H. Liew, Y. G. Rubo, and A. V. Kavokin, Phys. Rev. B **80**, 195309 (2009).
[35] I. L. Aleiner, B. L. Altshuler, and Y. G. Rubo, Phys. Rev. B **85**, 121301 (2012).

[36] C. Anton, T. C. H. Liew, G. Tosi, M. D. Martin, T. Gai, Z. Hatzopoulos, P. S. Eldridge, P. G. Savvidis, and L. Viña, Appl. Phys. Lett. **101**, 261116 (2012).
[37] T. C. H. Liew, A. V. Kavokin, and I. A. Shelykh, Phys. Rev. B **75**, 241301(R) (2007).
[38] C. Leyder, M. Romanelli, J. Ph. Karr, E. Giacobino, T. C. H. Liew, M. M. Glazov, A. V. Kavokin, G. Malpuech, and A. Bramati, Nat. Phys. **3**, 628 (2007).
[39] I. A. Shelykh, G. Pavlovic, D. D. Solnyshkov, and G. Malpuech, Phys. Rev. Lett. **102**, 046407 (2009).
[40] P. G. Savvidis, J. J. Baumberg, R. M. Stevenson, M. S. Skolnick, D. M. Whittaker, and J. S. Roberts, Phys. Rev. Lett. **84**, 1547 (2000).
[41] C. Ciuti, Phys. Rev. B **69**, 245304 (2004).
[42] O. A. Egorov and F. Lederer, Phys. Rev. B **87**, 115315 (2013).
[43] O. A. Egorov and F. Lederer, Opt. Lett. **39**, 4029 (2014).